

Degenerate Topological Edge States in Multimer Chains

Jun Li,^{1,2,*} Yaping Yang,^{1,†} and C.-M. Hu^{2,‡}

¹*MOE Key Laboratory of Advanced Micro-Structured Materials,*

School of Physics Science and Engineering, Tongji University, Shanghai, 200092, China

²*Department of Physics and Astronomy, University of Manitoba, Winnipeg R3T 2N2, Canada*
(Dated: June 6, 2023)

We propose and experimentally realize a class of quasi-one-dimensional topological lattices whose unit cells are constructed by coupled multiple identical resonators, with uniform hopping and inversion symmetry. In the presence of coupling-path-induced effective zero hopping within the unit cells, the systems are characterized by complete multimerization with degenerate -1 energy edge states for open boundary condition. Su-Schrieffer-Heeger subspaces with fully dimerized limits corresponding to pairs of nontrivial flat bands are derived from the Hilbert spaces. In particular, topological bound states in the continuum (BICs) are inherently present in even multimer chains, manifested by embedding the topological bound states into a continuous band assured by bulk-boundary correspondence. Moreover, we experimentally demonstrate the degenerate topological edge states and topological BICs in inductor-capacitor circuits.

Topological phases of matter transcend the paradigm of Ginzburg-Landau theory in condensed matter physics, with absence of any symmetry breaking but derived from geometry, and have attracted extensive investigation in various fields over the past few decades [1–9]. Topological phases are defined by the global wavefunctions of the dispersion bands that pervade the entire system rather than local orbitals, so that they are particularly robust to local perturbations such as defects and impurities. In essence, Band structure is the sufficient condition for the existence of topological phases. Since the first discovery of topological phases in quantum electronic systems [1, 2], novel and exotic topological properties have been developed in diverse platforms with their own unique advantages such as optics [10, 11], acoustics [12, 13], mechanics [14] and electric circuit [15–17] in classical regimes and ultra-cold atoms [18, 19], trapped-ions [20, 21] and Fock-state lattices [22, 23] in quantum regimes.

One-dimensional (1D) topological phases bring some new insights because of their manipulability and experimental accessibility. The Su-Schrieffer-Heeger (SSH) model of polyacetylene [24, 25], as a starting point for 1D topological models based on tight-binding approximation, is a dimerized chain by having two different alternating hopping amplitudes between nearest-neighbor lattice site hosts. Recently, in the context of SSH chains, a variety of extended configurations with new physics and phenomena has been proposed especially non-Hermitian topology [9, 26]. On the one hand, special inconsistent inter-site interactions, like periodically modulated hopping, nonreciprocal hopping, environment-induced coupling and multisite coupling, have been introduced to raise a plethora of distinct topological phenomena including but not limited to the non-Hermitian skin effect [27–31], non-Hermitian real spectra [32], dissipative and

Floquet topological phase transition [33–35] and trimer topological phases [36–39]. On the other hand, with respect to on-site potentials, the introduction of on-site gain and loss not only provides a pointcut to combine the non-Hermitianity and topological phases for widening topological family [40–42], but also can drive topologically trivial systems and induce topological phase transitions solely by deliberate design [43–47].

In this letter, we present a quasi-one-dimensional (quasi-1D) tight-binding configuration without any staggered hopping and on-site potentials. We consider unit cells of multiple identical resonators with uniform coupling between every two sites and the same strength as the inter-cell coupling, i.e., only one kind of coupling strength and resonators in the whole chain. The system then forms complete multimer due to the zero effective intracell hopping induced by special coupling paths. Conceivably, considering the bulk-boundary correspondence (BBC), degenerate topological edge states with full localization exist in finite systems [48]. Interesting, with the increase of resonators in the unit cell, pairs of nontrivial flat bands appear at two fixed frequencies which correspond to fully dimerized subspaces derived from the Hilbert spaces. Moreover, for even multimer chains, topological bound states in the continuum (BICs) [49] naturally form via the bandgap of nontrivial flat bands just covered by a trivial band. We experimentally implement the idea by using AC circuits consisting of uniform capacitors and inductors.

We start by considering a tight-binding system consisting of n ($n \geq 3$) identical resonators coupled to each other with the same hopping amplitude κ , as shown in Fig. 1 (a). Here, we consider an Hermitian system that the intrinsic and coupling losses of all the resonators are ignored and κ is sufficiently small compared to the frequency of resonators ω_0 . the systems can be represented by the Hamiltonian

* jli_phys@tongji.edu.cn

† yang_yaping@tongji.edu.cn

‡ hu@physics.umanitoba.ca

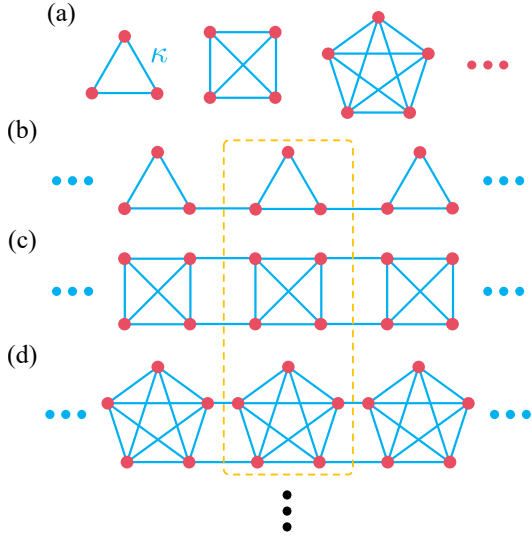


FIG. 1. Theoretical tight-binding hopping model. (a) Schematic of n ($n = 3, 4, 5 \dots$) resonators coupled with each others with uniform hopping amplitude κ . (b-d) Bulk model with n sites per unit cell, with uniform hoppings, unit cells framed in yellow dashed box.

$$H_n = \begin{pmatrix} 0 & \kappa & \kappa & \dots \\ \kappa & 0 & \kappa & \ddots \\ \kappa & \kappa & 0 & \ddots \\ \vdots & \ddots & \ddots & \ddots \end{pmatrix}_{n \times n}, \quad (1)$$

characterized that the diagonal elements of the matrix are zero and all the others are κ . Interestingly, there are always degenerate states with a fixed frequency independent of n in the system. Specifically, with reference to ω_0 , one of its eigenvalues is $\lambda_n = (n-1)\kappa$ with the normalized eigenvectors $|\psi_n\rangle = (1/\sqrt{n}, 1/\sqrt{n}, \dots, 1/\sqrt{n})'$ while the others are $\lambda_i = -\kappa$ where $i = 1, 2, \dots, n-1$ with the corresponding eigenvectors $|\psi_i\rangle = (0, \dots, 0, 1/\sqrt{2})'$ where the i th element $|\psi_i\rangle_i = 1/\sqrt{2}$. In terms of the splitting of eigenvalues, the local effective coupling between the degenerate modes can be seen as zero to some extent.

With this supposition, as shown in Figs 1 (b-d), we design a class of quasi-1D lattices with the above coupling multiple resonators as their unit cell. The unit cells are coupled to their nearest neighbor through $[n/2]$ independent coupling channels with the same hopping amplitudes κ . Considering the zero effective intracell hopping, we can expect that our chains are topologically nontrivial with complete mimerization. In bulk momentum space, the Bloch Hamiltonian of the chain can be written

as

$$H_n(k) = \begin{pmatrix} 0 & \kappa & \dots & \kappa + \kappa e^{-ika} \\ \kappa & 0 & \ddots & \kappa \\ \vdots & \ddots & \ddots & \vdots \\ \kappa + \kappa e^{ika} & \kappa & \dots & 0 \end{pmatrix}_{n \times n} \quad (2)$$

where a is the lattice constant between the units and k is the Bloch wave number. The Bloch Hamiltonian shows that the Bloch term only exists in all anti-diagonal elements, provided that the diagonal term remains zero. Obviously, the Hamiltonian displays inversion (\mathcal{I}) symmetry, i.e., $\mathcal{I}H_n(k)\mathcal{I}^{-1} = H_n(-k)$. For clarity, the system is classified into two patterns via n is odd or even in the following analysis. We find the analytical solutions of its energy spectra expressed as

$$\omega_{n,o}(k) = \begin{pmatrix} -2 \\ \vdots \\ n/3 - 1 - (A_+ + i\sqrt{3}A_-)/2 \\ n/3 - 1 - (A_+ - i\sqrt{3}A_-)/2 \\ 0 \\ \vdots \\ n/3 - 1 + A_+ \end{pmatrix} \kappa \quad (3)$$

when n is odd where $A_{\pm} = C/B \pm B$, $B = [\sqrt{D^2 - C^3} + D]^{1/3}$, $C = (n-1)\cos ka/3 + (n^2+3)/9$ and $D = (n^2-n)\cos ka/6 + (n/3)^3 + (n-3)/6$. Surprisingly, there are $n-3$ flat bands equally divided at $\omega_n = 0$ and $\omega_n = -2\kappa$. And only two bandgaps with the width $G_1 = \sqrt{(n-2)^2+1} - \sqrt{(n-1)^2-1} + 1$ and $G_2 = \sqrt{(n-2)^2+1} + n-2$ exist in the energy spectra. For the case where n is even, the eigenfrequency is given by

$$\omega_{n,e}(k) = \begin{pmatrix} -2 \\ \vdots \\ n/2 - 1 - \sqrt{n^2/4 + 1 + n \cos ka} \\ 0 \\ \vdots \\ n/2 - 1 + \sqrt{n^2/4 + 1 + n \cos ka} \end{pmatrix} \kappa, \quad (4)$$

characterized by having $n/2-1$ flat bands at $\omega_n = 0$ and $\omega_n = -2\kappa$ respectively. The $(n/2)$ th band and the top (n th) band are symmetric with respect to $(n/2-1)\kappa$. It is noteworthy that as the parameter n varies, there consistently exists one bandgap with a width of $G = n-2$ due to the lower non-flat band precisely overlapping the bandgap of the flat bands. In both cases, the band structure of the bulk Hamiltonian is not symmetric around zero, indicating that our chain is chiral symmetry broken. In detail, except for the top band that exceeds zero, the other bands are always distributed between -2κ and zero.

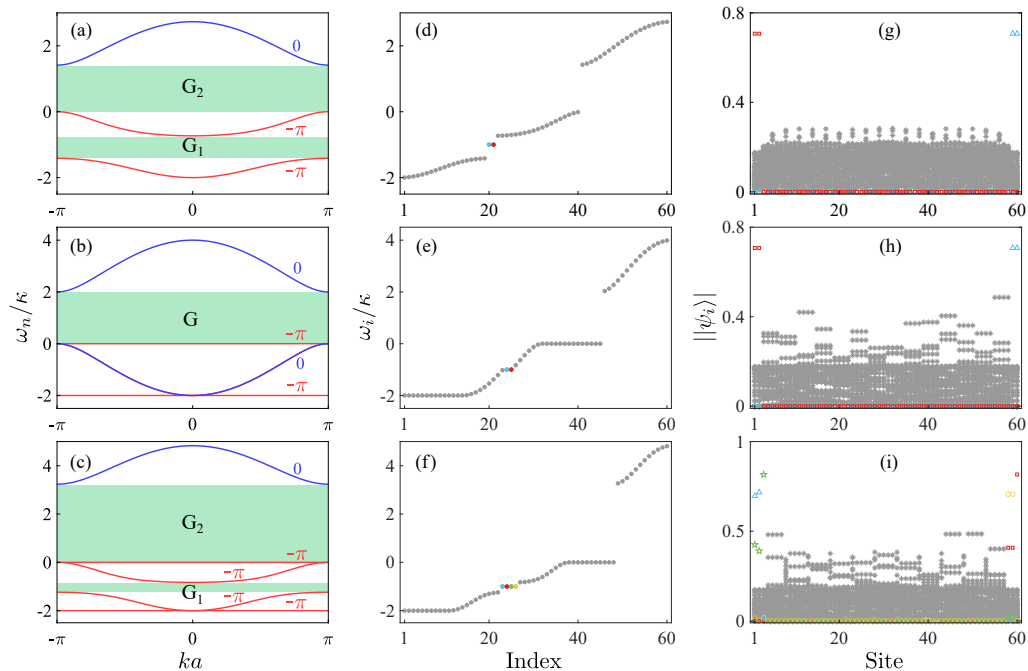


FIG. 2. Topological edge states of multimer chains. (a-c) The normalized band structures with quantized Zak phases and (d-f) sorted eigenvalues of topological finite chains (composed of 60 resonators) with (g-i) corresponding representative wave functions for (a, d, g) $n = 3$, (b, e, h) $n = 4$ and (c, f, i) $n = 5$, respectively. Zak phases for the bands labeled by red are $-\pi$ and 0 by blue in (a-c). The edge and bulk states in (d-f) with the corresponding intensity distributions in (g-i) are represented by color and gray, respectively. Particularly, the wavefunction distributions in panels (h) and (i) represent individual instances of potential numerical solutions for $n = 4$ and $n = 5$, respectively.

Figures 2 (a-c) show the band structures in first Brillouin zone for different n . Here, in the presence of inversion symmetry, we introduce the Zak phase, defined as $Z_j = -i \int_{-\pi/a}^{\pi/a} \langle \psi_{k,j} | \partial_k | \psi_{k,j} \rangle dk$, to characterize the topology of our 1D multimer system where j specifies the occupied band index with corresponding Bloch wave functions $|\psi_{k,j}\rangle$ [50]. We can obtain nonzero quantized Zak phases of bands for various n , indicating the topological nontriviality of our chains. Particularly, the top band possesses a Zak phase of zero while the flat bands always have Zak phases of $-\pi$. We can block-diagonalize $H_n(k)$ by unitary transformation $\mathcal{U}_n^{-1} H_n(k) \mathcal{U}_n = H_n^{BD}(k)$ to show the separation between flat and nonflat bands clearly. For the simplest case with $n = 4$, the unitary matrix and the block-diagonal Hamiltonian are

$$\mathcal{U}_4 = \frac{1}{\sqrt{2}} \begin{pmatrix} 1 & 0 & 1 & 0 \\ 1 & 0 & -1 & 0 \\ 0 & 1 & 0 & -1 \\ 0 & 1 & 0 & 1 \end{pmatrix}, \quad (5)$$

$$H_4^{BD}(k) = \begin{pmatrix} 1 & 2 + e^{-ika} & 0 & 0 \\ 2 + e^{ika} & 1 & 0 & 0 \\ 0 & 0 & -1 & e^{-ika} \\ 0 & 0 & e^{ika} & -1 \end{pmatrix} \kappa, \quad (6)$$

respectively. As expected, the both 2×2 blocks have the same form as the SSH Hamiltonian where the upper one

is topologically trivial corresponding to the blue bands and the lower block is topologically nontrivial with complete dimerization corresponding to the flat bands. More generally, the bulk Hamiltonians for larger n can be divided into a topological trivial dimerized subspace and $n/2 - 1$ nontrivial fully dimerized subspaces by the unitary transformation when n is even. Moreover, the lower trivial band for even chain always spans the bandgap between the flat bands by meeting the upper and lower flat bands at the boundary and center of the first Brillouin zone, respectively. Similarly, for odd n , we can get the block-diagonal Hamiltonian composed of a 3×3 block and $(n-3)/2$ same nontrivial 2×2 blocks (see Supplemental Material for details [51]) where the 3×3 subspace owns two nontrivial lower bands in contact with the upper and lower flat bands independently.

Considering the BBC, under the open boundary condition, we show the normalized eigenvalue spectra ω_i/κ of finite multimer chains with 60 resonators in Figs. 2 (d-f) and the corresponding wave functions $|\psi_i\rangle$ in Figs. 2 (g-i) for $n = 3, 4$ and 5 . Mathematically, the wavefunction solution is not unique for the finite-size chains with $n > 3$, owing to the fact that the rank of the Hamiltonian matrix is smaller than the matrix dimension. The wavefunction distributions depicted in Figs. 2 (h) and 2 (i) exemplify potential numerical solutions for $n = 4$ and $n = 5$, respectively. Correspondingly, there are pairs of degenerate edge states marked by the colored dots at

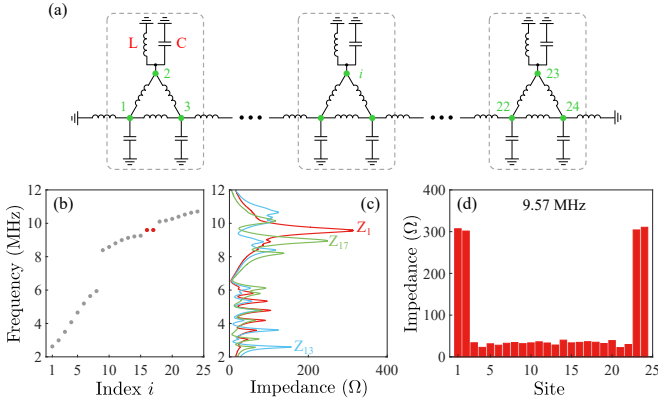


FIG. 3. Observation of topological edge states in trimer chain. (a) Circuit diagram of the finite experimental trimer chain, unit cells consists of three capacitors C with identical inductors L between every two capacitors framed in grey dashed boxes. (b) Calculated admittance eigenspectrum of the LC circuit for $C = 1$ nF and $L = 1.1$ μ H. (c) Measured impedances between the nodes ($|Z_1|$, $|Z_{13}|$ and $|Z_{17}|$) and ground vs the frequency of circuit. (d) Location distribution of impedance at the frequency $f = 9.57$ MHz.

the exact detuning $-\kappa$ with the same number as the non-trivial bands. The topological edge modes of odd multimer chain sit in the lower bandgap G_1 . Remarkably, the topological edge states are clearly embedded in the continuous spectrum of the lower nontrivial band and are the so-called topological BICs [49] when n is even. Because of the complete multimerization, the wave functions of exact -1 energy edge modes are absolutely localized at the two boundary cells without any distribution in the bulk, while the bulk wave functions are diffused throughout the whole chains.

We employ periodic inductor-capacitor (LC) circuits featuring flexible hopping channels to experimentally observe the tight-binding modes. Here, the lattice nodes are capacitively coupled to ground and inductively coupled to each other. The multimer chains can be represented by the admittance matrix J_ω (also termed circuit Laplacian) [17, 42]. The voltage response $\mathbf{V}(\omega)$ of the nodes to a input current $\mathbf{I}(\omega)$ at frequency ω follows Kirchhoff's law: $\mathbf{I}(\omega) = J(\omega)\mathbf{V}(\omega)$ where the vectors $\mathbf{I}(\omega) = [I_1, I_2, \dots, I_s]'$ and $\mathbf{V}(\omega) = [V_1, V_2, \dots, V_s]'$ for s nodes circuit. For our uniform hopping chains, using the same size capacitors C and inductors L , we have the circuit Laplacian

$$J(\omega) = \frac{1}{i\omega} \left[\left(\frac{n}{L} - \omega^2 C \right) \mathbb{I} + H \right] \quad (7)$$

with

$$H = \begin{pmatrix} 0 & -1/L & -1/L & \dots \\ -1/L & 0 & -1/L & \dots \\ -1/L & -1/L & 0 & \dots \\ \vdots & \vdots & \vdots & \ddots \end{pmatrix}_{s \times s}, \quad (8)$$

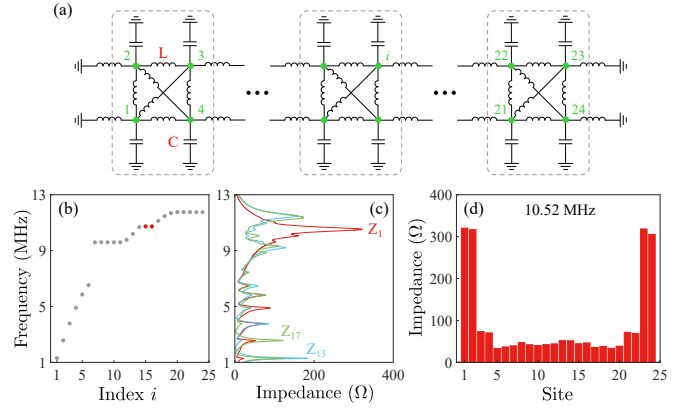


FIG. 4. Observation of topological BICs in tetramer chain. (a) Circuit diagram blueprint with unit cells framed in grey dashed boxes. (b) Calculated admittance eigenvalues of the tetramer LC circuit for $C = 1$ nF and $L = 1.1$ μ H. (c) Frequency scan of measured impedances for representative edge ($|Z_1|$) and bulk ($|Z_{13}|$ and $|Z_{17}|$) nodes. (d) Impedance distribution of topological edge mode at the frequency $f = 10.52$ MHz.

where \mathbb{I} is the $s \times s$ unit matrix and H can represent our theoretical model accurately with the hopping amplitude $-1/L$. We construct periodic LC circuits with 24 nodes for trimer and tetramer configurations as shown in Fig. 3 (a) and Fig. 4 (a), respectively. By solving the eigenvalues E_i of H numerically, we can obtain the general admittance eigenspectra dispersion as $f_i = \sqrt{(n/L + E_i)/C}/(2\pi)$ with degenerate edge states labeled by red shown in Figs. 3 (b) and 4 (b). Note that the inverted nonlinear spectra is due to the negative frequency-dependent hopping amplitude of inductive coupling.

In the experiment implementation, we choose the circuit components: $C = 1$ nF with $\pm 1\%$ tolerance and $L = 1.1$ μ H with $\pm 5\%$ deviation. Details of the sample fabrication and impedance measurements are provided in the Supplemental Material [51]. Measured impedances of nodes 1, 13, and 17 to ground ($|Z_1|$, $|Z_{13}|$ and $|Z_{17}|$) versus the frequency of input circuit are shown in Fig. 3 (c) and Fig. 4 (c) for trimer and tetramer chain, respectively. The peak frequencies of the impedances are in good agreement with the calculated eigenvalues, despite some slight frequency shift of the measured impedance peaks due to component tolerances. In Fig. 3 (c), the highest impedance peak near 9.57 MHz of edge node inside the band gap (about 9.25 - 10.1 MHz) with impedance valleys for bulk nodes denotes the topological modes unambiguously. More intuitively, We measure the impedance distribution of the degenerate topological edge modes with strong locality at both ends at 9.57 MHz shown in Fig. 3 (d). Differently, in Fig. 4 (c), the impedance peak of edge node is accompanied by the impedance peaks of the bulk nodes near the frequency of edge state 10.52 MHz, representing the existence of a topological bound state in a nontopological continuum where the bound edge state

are show in Fig. 4 (d).

In summary, we theoretically and experimentally demonstrated degenerate topological edge states in a class of topological multimer chains consisting of identical resonators with uniform hopping. By designing deliberate coupling paths, the systems exhibit full multimerization with fully dimerized SSH subspaces corresponding to flat bands that can be separated from their Hilbert spaces. We also show topological BICs by embedding the degenerate topological bound states into a continuous band in even chains naturally. Our scheme is experimental accessible and can also be implemented in coupled

waveguides arrays [39, 52], optical and acoustic coupled cavity arrays [49, 53], cold atoms lattices [54] and three-dimensional circuit quantum electrodynamics [55]. Our work sheds new light on the construction of topological phases.

This work is supported by National Key Research and Development Program of China (2021YFA1400600, 2021YFA1400602), the NSERC Discovery Grants and NSERC Discovery Accelerator Supplements (C.-M. H.), the National Natural Science Foundation of China (12274326) and China Scholarship Council (202106260079).

-
- [1] K. v. Klitzing, G. Dorda, and M. Pepper, *Phys. Rev. Lett.* **45**, 494 (1980).
- [2] D. J. Thouless, M. Kohmoto, M. P. Nightingale, and M. den Nijs, *Phys. Rev. Lett.* **49**, 405 (1982).
- [3] F. D. M. Haldane, *Phys. Rev. Lett.* **61**, 2015 (1988).
- [4] M. Z. Hasan and C. L. Kane, *Rev. Mod. Phys.* **82**, 3045 (2010).
- [5] X.-L. Qi and S.-C. Zhang, *Rev. Mod. Phys.* **83**, 1057 (2011).
- [6] A. Bansil, H. Lin, and T. Das, *Rev. Mod. Phys.* **88**, 021004 (2016).
- [7] C.-K. Chiu, J. C. Y. Teo, A. P. Schnyder, and S. Ryu, *Rev. Mod. Phys.* **88**, 035005 (2016).
- [8] X.-G. Wen, *Rev. Mod. Phys.* **89**, 041004 (2017).
- [9] E. J. Bergholtz, J. C. Budich, and F. K. Kunst, *Rev. Mod. Phys.* **93**, 015005 (2021).
- [10] L. Lu, J. D. Joannopoulos, and M. Soljačić, *Nature Photonics* **8**, 821 (2014).
- [11] T. Ozawa, H. M. Price, A. Amo, N. Goldman, M. Hafezi, L. Lu, M. C. Rechtsman, D. Schuster, J. Simon, O. Zeitlinger, and I. Carusotto, *Rev. Mod. Phys.* **91**, 015006 (2019).
- [12] Z. Yang, F. Gao, X. Shi, X. Lin, Z. Gao, Y. Chong, and B. Zhang, *Phys. Rev. Lett.* **114**, 114301 (2015).
- [13] M. Xiao, G. Ma, Z. Yang, P. Sheng, Z. Q. Zhang, and C. T. Chan, *Nature Physics* **11**, 240 (2015).
- [14] S. D. Huber, *Nature Physics* **12**, 621 (2016).
- [15] V. V. Albert, L. I. Glazman, and L. Jiang, *Phys. Rev. Lett.* **114**, 173902 (2015).
- [16] J. Ningyuan, C. Owens, A. Sommer, D. Schuster, and J. Simon, *Phys. Rev. X* **5**, 021031 (2015).
- [17] C. H. Lee, S. Imhof, C. Berger, F. Bayer, J. Brehm, L. W. Molenkamp, T. Kiessling, and R. Thomale, *Communications Physics* **1**, 39 (2018).
- [18] N. R. Cooper, J. Dalibard, and I. B. Spielman, *Rev. Mod. Phys.* **91**, 015005 (2019).
- [19] J. Perczel, J. Borregaard, D. E. Chang, H. Pichler, S. F. Yelin, P. Zoller, and M. D. Lukin, *Phys. Rev. Lett.* **119**, 023603 (2017).
- [20] N. Hao and J. Hu, *National Science Review* **6**, 213 (2018).
- [21] P. T. Dumitrescu, J. G. Bohnet, J. P. Gaebler, A. Hankin, D. Hayes, A. Kumar, B. Neyenhuis, R. Vasseur, and A. C. Potter, *Nature* **607**, 463 (2022).
- [22] H. Cai and D.-W. Wang, *National Science Review* **8**, 10.1093/nsr/nwaa196 (2020).
- [23] J. Deng, H. Dong, C. Zhang, Y. Wu, J. Yuan, X. Zhu, F. Jin, H. Li, Z. Wang, H. Cai, C. Song, H. Wang, J. Q. You, and D.-W. Wang, *Science* **378**, 966 (2022).
- [24] W. P. Su, J. R. Schrieffer, and A. J. Heeger, *Phys. Rev. Lett.* **42**, 1698 (1979).
- [25] A. J. Heeger, S. Kivelson, J. R. Schrieffer, and W. P. Su, *Rev. Mod. Phys.* **60**, 781 (1988).
- [26] K. Kawabata, K. Shiozaki, M. Ueda, and M. Sato, *Phys. Rev. X* **9**, 041015 (2019).
- [27] T. E. Lee, *Phys. Rev. Lett.* **116**, 133903 (2016).
- [28] S. Yao and Z. Wang, *Phys. Rev. Lett.* **121**, 086803 (2018).
- [29] F. Song, S. Yao, and Z. Wang, *Phys. Rev. Lett.* **123**, 246801 (2019).
- [30] N. Okuma, K. Kawabata, K. Shiozaki, and M. Sato, *Phys. Rev. Lett.* **124**, 086801 (2020).
- [31] *Nature Physics* **16**, 747 (2020).
- [32] Y. Long, H. Xue, and B. Zhang, *Phys. Rev. B* **105**, L100102 (2022).
- [33] W. Nie, M. Antezza, Y.-x. Liu, and F. Nori, *Phys. Rev. Lett.* **127**, 250402 (2021).
- [34] C. Fan, X. Shi, F. Wu, Y. Li, H. Jiang, Y. Sun, and H. Chen, *Photon. Res.* **10**, 41 (2022).
- [35] M. Jangjan, L. E. F. Foa Torres, and M. V. Hosseini, *Phys. Rev. B* **106**, 224306 (2022).
- [36] W. P. Su and J. R. Schrieffer, *Phys. Rev. Lett.* **46**, 738 (1981).
- [37] V. M. Martinez Alvarez and M. D. Coutinho-Filho, *Phys. Rev. A* **99**, 013833 (2019).
- [38] M. Jangjan and M. V. Hosseini, *Scientific Reports* **11**, 12966 (2021).
- [39] W. Yan, W. Cheng, W. Liu, and F. Chen, *Opt. Lett.* **48**, 1802 (2023).
- [40] S. Weimann, M. Kremer, Y. Plotnik, Y. Lumer, S. Nolte, K. G. Makris, M. Segev, M. C. Rechtsman, and A. Szameit, *Nature Materials* **16**, 433 (2017).
- [41] W. Song, W. Sun, C. Chen, Q. Song, S. Xiao, S. Zhu, and T. Li, *Phys. Rev. Lett.* **123**, 165701 (2019).
- [42] A. Stegmaier, S. Imhof, T. Helbig, T. Hofmann, C. H. Lee, M. Kremer, A. Fritzsche, T. Feichtner, S. Klemmt, S. Höfling, I. Boettcher, I. C. Fulga, L. Ma, O. G. Schmidt, M. Greiter, T. Kiessling, A. Szameit, and R. Thomale, *Phys. Rev. Lett.* **126**, 215302 (2021).
- [43] K. Takata and M. Notomi, *Phys. Rev. Lett.* **121**, 213902 (2018).
- [44] X.-W. Luo and C. Zhang, *Phys. Rev. Lett.* **123**, 073601 (2019).
- [45] H. Gao, H. Xue, Q. Wang, Z. Gu, T. Liu, J. Zhu, and

- B. Zhang, *Phys. Rev. B* **101**, 180303 (2020).
- [46] H. Xue, Q. Wang, B. Zhang, and Y. D. Chong, *Phys. Rev. Lett.* **124**, 236403 (2020).
- [47] J.-R. Li, L.-L. Zhang, W.-B. Cui, and W.-J. Gong, *Phys. Rev. Res.* **4**, 023009 (2022).
- [48] J. Asbóth, L. Oroszlány, and A. Pályi, *A Short Course on Topological Insulators: Band Structure and Edge States in One and Two Dimensions*, Lecture Notes in Physics (Springer International Publishing, 2016).
- [49] Y.-X. Xiao, G. Ma, Z.-Q. Zhang, and C. T. Chan, *Phys. Rev. Lett.* **118**, 166803 (2017).
- [50] J. Zak, *Phys. Rev. Lett.* **62**, 2747 (1989).
- [51] See supplemental material for the details of experimental setup, admittance formalism and subspace decomposition.
- [52] Z.-Q. Jiao, S. Longhi, X.-W. Wang, J. Gao, W.-H. Zhou, Y. Wang, Y.-X. Fu, L. Wang, R.-J. Ren, L.-F. Qiao, and X.-M. Jin, *Phys. Rev. Lett.* **127**, 147401 (2021).
- [53] Z. Guo, J. Jiang, H. Jiang, J. Ren, and H. Chen, *Phys. Rev. Res.* **3**, 013122 (2021).
- [54] N. Goldman, G. Juzeliūnas, P. Öhberg, and I. B. Spielman, *Reports on Progress in Physics* **77**, 126401 (2014).
- [55] W. Nie, Z. H. Peng, F. Nori, and Y.-x. Liu, *Phys. Rev. Lett.* **124**, 023603 (2020).